

Evaluation of Flow Accelerated Corrosion in Typical Recovery Boiler Environments of Energy Production Industries

Rogaciano M. Moreira^a, Tatiana C. Almeida^{a,b*} , Merlin C. E. Bandeira^a ,
Felipe R. S. Assunção^a, Juliana F. A. Carvalho^a, Elaine F. Silva^a, João V. T. Verbicario^a,
Oscar R. Mattos^a, Jefferson R. Oliveira^c, André L. C. Bonfim^c, André R. Novgorodecev^c 

^aUniversidade Federal do Rio de Janeiro (UFRJ), Laboratório de Ensaios Não Destrutivos, Corrosão e Soldagem (LNDC/COPPE), 21941-596, Rio de Janeiro, RJ, Brasil.

^bUniversidade Federal Fluminense (UFF), Escola de Engenharia Industrial Metalúrgica de Volta Redonda, 27255-125, Volta Redonda, RJ, Brasil.

^cPetrobras, Centro de Pesquisas, Desenvolvimento e Inovação (CENPES), Cidade Universitária, 21941-915, Rio de Janeiro, RJ, Brasil.

Received: October 06, 2021; Revised: March 06, 2022; Accepted: March 07, 2022

Flow accelerated corrosion (FAC) is a steel degradation that occurs in heat recovery steam generators in the power industry. The mechanism of this corrosion comprises an electrochemical dissolution of the semi-protective magnetite layer (Fe_3O_4) that is formed within the pipes employed in the boilers. The FAC is influenced by different factors such as fluid velocity, pH and dissolved oxygen concentration. In this context, Rotating Cage tests were used to evaluate the influence of pH and dissolved oxygen content on FAC of A210, P11 and P22 steels. General corrosion was lower for P11 and P22 steels, an effect consistent with the presence of chromium in their compositions. General corrosion was most critical at pH 8.5. The corrosion intensity decreased for the three steels when the dissolved oxygen concentration increased, at 2 m/s. This behavior is coherent considering the most effective precipitation of Fe_2O_3 inside the pores of the Fe_3O_4 layer in a more oxidizing environment. For 3 m/s, the corrosion intensity increased for both materials when oxygen increased, showing the shear stress effect. These behaviors were more significant at pH 8.5. About pitting corrosion, the analyzes show localized attack in the majority of coupons, however with very low number of pits.

Keywords: FAC, Rotating Cage, Carbon Steel, Magnetite Layer.

1. Introduction

In the energy industry, many equipment is degraded over time and conditions of use. In Heat Recovery Steam Generators (HRSG), boilers present in thermoelectric power plants, about 40% of pipeline failures occur due to Flow Accelerated Corrosion (FAC)^{1,2}. The FAC is a phenomenon observed mainly in carbon steels and less frequently in low-alloy steels, which results in a decrease in the thickness of tubes and vessels exposed to water or water vapor flows. The consequence of this type of corrosion is the appearance of a failure in equipment built with these materials. Parameters such as pH, dissolved oxygen concentration, fluid velocity, material composition, temperature, presence of reducing agents, oxidation-reduction potential and geometric configuration of the components, have been identified as parameters that have influence on the FAC process²⁻¹⁸.

The internal surfaces of the pipes used in boilers are often covered by a semi-protective layer of magnetite (Fe_3O_4). In Flow accelerated corrosion, the steel degradation

mechanism occurs due to the electrochemical dissolution of magnetite, accelerated by the presence of a flow of water (single-phase) or water vapor (two-phase) with normally turbulent regime¹². This process decreases the thickness of the semi-protective oxide layer or eliminates it, and since magnetite is constantly formed from the anodic dissolution of carbon steel, there is an increase on steel corrosion rate. This process is quite common for temperatures close to 150 °C¹⁵, when the magnetite layers are more porous and less adherent, which allows a more severe corrosion of the tube wall, which can result in failures.

A study of the effect of oxygen concentration, linear velocity of the corrosive environment and pH was carried out to evaluate the FAC in A210, P11 and P22 steels, using a Rotating Cage system. These steels are commonly used in the tubes of the recovery boilers of Thermoelectric Plants powered by natural gas, and where FAC normally occurs. From the results presented herein, a better understanding of the impact of those parameters on FAC corrosion is essential for adjustments in water chemistry and steels specification to minimize the Flow Accelerated Corrosion in those systems.

*e-mail: tatianachagas@id.uff.br

2. Experimental Methodology

The Rotating Cage (RC) tests were performed in *Cortest* Hastelloy C-276 autoclaves 5L. A schematic drawing of the system is shown in Figure 1. The system consists of the autoclave containing the RC made of PEEK, a reservoir with deionized water, a sampling cell, to evaluate the conductivity of the environment, pH and concentration of dissolved oxygen, and gas cylinders used to pressurize the autoclave. A picture of the system is shown in Figure 2. Moreover, coolers were installed at the autoclave gases out, to avoid water losses during the tests, and at the entrance of the sampling cell, to measure the parameters at room temperature. The autoclave was adapted to carry out tests at high velocity, allowing rotations of up to 2,750 rpm, enabling linear velocities of up to 11 m/s. A vortex breaker was used to eliminate this phenomenon from the tests.

Figure 3 shows the Rotating Cage before assembling the autoclave, with the cage connected to autoclave lid stirring system (A) and with samples installed in the Cage (B).

The tests were performed with A-210, P11 and P22 steel coupons, with dimensions of 20 mm x 30 mm x 2 mm and a surface finish equivalent to # 600. The steel chemical compositions are shown in Table 1.

After cleaning with water and acetone, all samples were air-dried, measured and weighed with an analytical balance (0.1 mg). The Rotating Cage was assembled with 3 coupons of steel A-210, 3 of P11 and 2 of P22.

All tests were performed with ultrapure water. The complete system, including water, was deaerated with N_2 (99.999%) and the absence of dissolved O_2 was evaluated by sampling the water before transferring it to the autoclave, using Dissolved O_2 sensor Mettler Toledo Optical InPro 6970i. The parameters used in the tests are shown in Table 2. For tests with different levels of dissolved oxygen, gas

mixtures composed of oxygen and nitrogen were used, in order to obtain the O_2 concentrations dissolved in water at 8 $\mu\text{g/L}$ and 50 $\mu\text{g/L}$. For O_2 -free tests, the system was maintained under constant N_2 saturation.

After conditioning the autoclave at test temperature and pressure, the pH was adjusted with the addition of ammonium hydroxide (NH_4OH) which was injected directly into the autoclave with metering pump. The pH adjustment was monitored by sampling at the beginning of the tests. These samples were also used to evaluate whether the water initial conductivity was within the required limit. For low conductive environments, these parameters were measured with appropriate equipment, such as pH meter Mettler Toledo InLab Pure Pro ISM and Conductivity meter Mettler Toledo InLab 742 ISM.

The autoclave was filled with 4,500 mL of water and the stirrer rotation was activated after reaching the temperature, pressure and pH conditions of the tests. A flow of 50 mL/min of N_2 or N_2/O_2 was maintained throughout the test.

After the immersion corrosion tests, weight loss tests were performed according to ASTM G1¹⁹ procedures. The steel coupons were analyzed by 3D confocal microscopy, using a Zeiss AXIO CSM 700 confocal microscope. Furthermore, a surface analyses of carbon steel coupons before the weight loss were performed using a Bruker SENTERRA Raman confocal microscope with the excitation line of 532 nm, 2 mW laser power focalized on the sample with an Olympus 20x long-working distance objective and spectral resolution of 3 – 5 cm^{-1} .

3. Results and Discussions

3.1. General corrosion

The steel coupons general corrosion was evaluated after the RC immersion test under specific flow conditions by

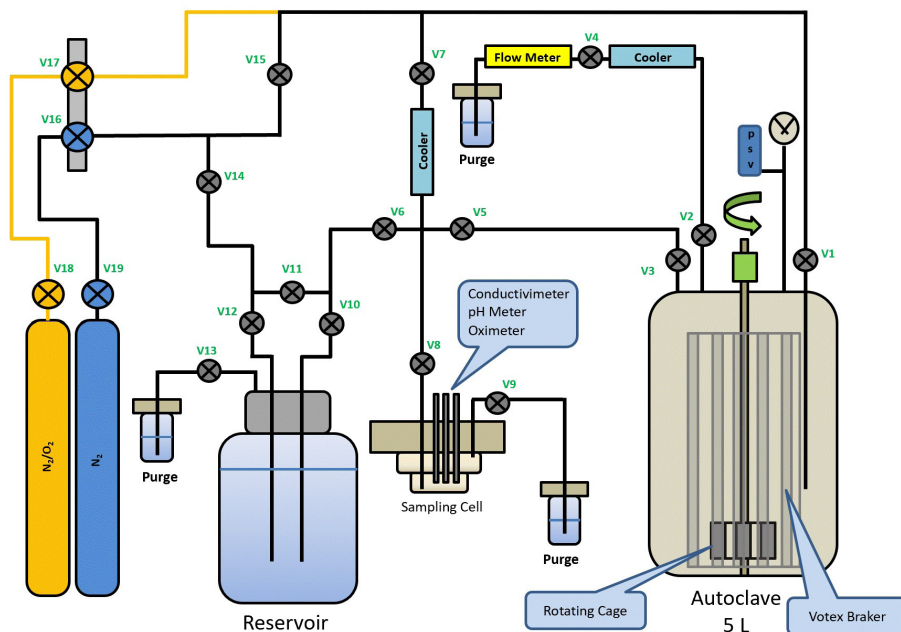


Figure 1. Schematic drawing used to assemble the Flow Accelerated Corrosion system.



Figure 2. Image of the system used in the Flow Accelerated Corrosion procedures.

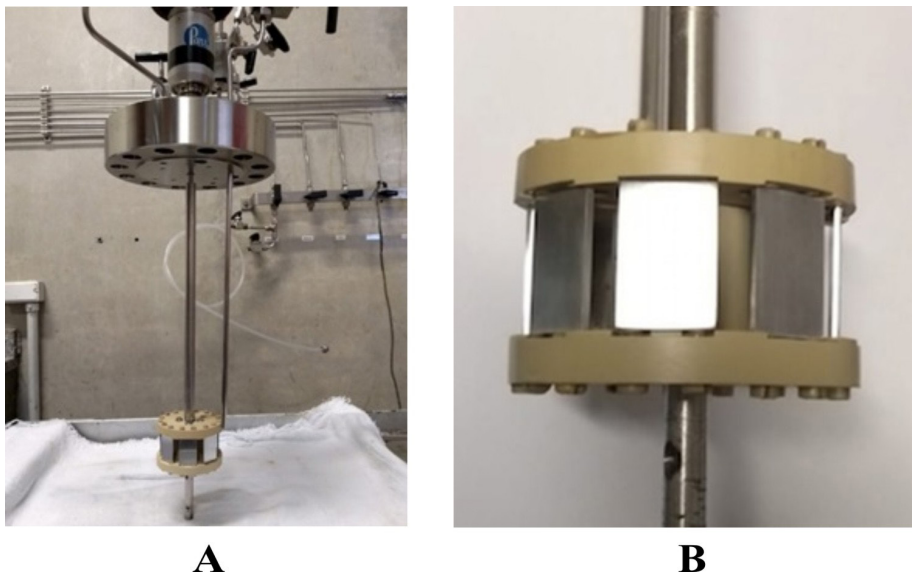


Figure 3. Images of the Rotating Cage system A) with the cage connected to the autoclave lid stir system and B) with the test coupons installed in the Cage.

Table 1. Nominal chemical composition of the steels (wt %).

Aço	C	Mn	Si	P	S	Cr	Mo
A-210	0.21	0.53	0.27	0.022	0.002	0.03	0.00
P11	0.11	0.41	0.57	0.008	0.001	1.06	0.46
P22	0.05/0.15	0.30/0.60	0.50 (max.)	0.025 (max.)	0.025 (max.)	1.90/2.60	0.87/1.13

Source: Steel supplier.

weight loss tests according to ASTM G1¹⁹. Table 3 shows the general corrosion rates obtained for A-210, P11 and P22 steels in the different environments studied. Each value was determined by the average of results from three coupons, and can be seen in the graphs in Figure 4 together with the results of dispersion values. A general analysis shows that the corrosion rates increased in the following order: A-210 > P11 > P22. The highest corrosion rate obtained was 0.613 mm/year for the A-210, tested in the condition of 3 m/s - pH 8.5 - 50 µg/L O₂. This result reflects an expected behavior, since A-210 does not have the chromium element in its composition, P11 has ca. 1% Cr and P22 has ca. 2% Cr, showing, therefore, the effect of this element in the protection against general corrosion (Table 1). Additionally, the highest corrosion rates were found on coupons tested at pH 8.5, mainly for environments containing dissolved O₂. This behavior is coherent with the tendency of these steels to reduce corrosion rates when the pH is increased, due to the decreased solubility of the semi protective magnetite film present. In O₂-free environments, the corrosion rates

were relatively low and did not vary significantly with pH. A-210 presented the highest corrosion rate values for these conditions, at 2 m/s.

Figure 4 shows the behavior of general corrosion rates (FAC rates) as a function of the dissolved O₂ concentrations according to the studied pH and velocities. It is quite clear the decrease in corrosion rates of all conditions with increasing pH and no relevant variation in O₂-free conditions. At 2 m/s and pH 8.5 (Figure 4A) there is an increase in the corrosion rate when the system changes to 8 µg/L O₂, reaching ca. 0.22 mm/year for A-210, followed by a decrease to ca. 0.12 mm/year at 50 µg/L O₂. This behavior is accompanied by other types of steel, but with lower corrosion rates, and may be associated with the process of the Fe₂O₃ formation during the exposure of steel to the corrosive environment containing O₂, as reported in the literature^{2,3,5,15}. These oxides help to protect the steel by filling the pores of the semi-protective magnetite film (Fe₃O₄), previously formed on the steel, reducing the diffusion of ferrous ions from the oxidation of the metal to the oxide/water interface. This process is favored by the presence of a higher concentration of O₂ dissolved in solution and also by the lower solubility of these oxides, if compared with the magnetite^(2,3). When the linear velocity is increased to 3 m/s at the same pH (Figure 4B), the corrosion rates increase when the O₂ concentration reaches 50 µg/L, differently from that observed at 2 m/s. Corrosion rates ca. 0.61 mm/year were obtained for A-210 steel and similar behavior was observed for P11 and P22 steels, however with smaller magnitudes. In this case, there may be a synergistic effect of the higher shear stress and a more oxidizing environment, with a higher concentration of O₂, making it difficult to stabilize the magnetite pore closure process by the formation of Fe₂O₃, hence increasing corrosion rates with dissolved O₂ content. This behavior is in agreement with that reported in the literature, with the electrochemical dissolution of magnetite accelerated by the presence of a water flow, FAC¹².

Table 2. Test parameters.

Parameter	Magnitude
Water conductivity (µS/cm)*	0.2
pH	8.5; 9.5; 10
Dissolved oxygen (µg/L)	0; 8; 50
NH ₄ OH (%)	Amount needed for pH control
Hydrazine (%)	Amount needed for pH and O ₂ control
Pressure (Bar)	10
Cage rotation (rpm)	480; 710
Linear velocity (m/s)	2.0; 3.0
Temperature (°C)	150
Duration (day)	7

*Maximum required at the beginning of the tests.

Table 3. Average corrosion rate for A-210, P11 and P22 steels exposed to FAC conditions with pH 8.5, pH 9.5 and pH 10, at linear velocities of 2 m/s and 3 m/s.

Testing Condition	Corrosion Rates (mm/year)					
	2 m/s			3 m/s		
	A-210	P11	P22	A-210	P11	P22
0 µg/L O ₂ - pH 8.5	0.053	0.022	0.015	0.013	0.012	0.013
8 µg/L O ₂ - pH 8.5	0.218	0.131	0.094	0.117	0.108	0.056
50 µg/L O ₂ - pH 8.5	0.126	0.053	0.033	0.613	0.426	0.303
0 µg/L O ₂ - pH 9.5	0.030	0.016	0.013	0.019	0.017	0.014
8 µg/L O ₂ - pH 9.5	0.079	0.048	0.053	0.082	0.075	0.032
50 µg/L O ₂ - pH 9.5	0.067	0.094	0.038	0.087	0.037	0.016
0 µg/L O ₂ - pH 10	0.055	0.017	0.018	0.012	0.013	0.012
8 µg/L O ₂ - pH 10	0.009	0.010	0.007	0.027	0.018	0.017
50 µg/L O ₂ - pH 10	0.012	0.014	0.010	0.037	0.030	0.024

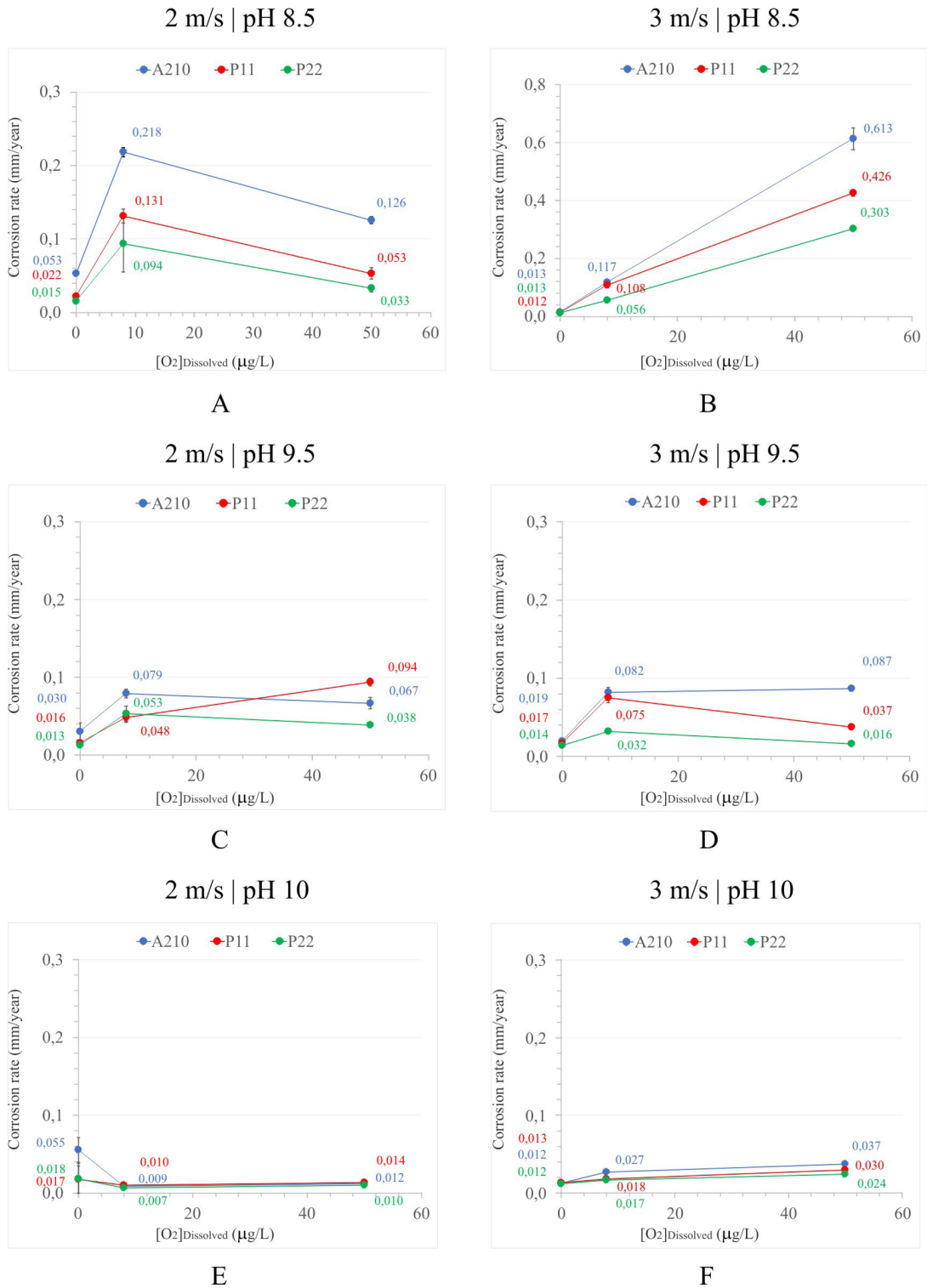


Figure 4. Behavior of the average corrosion rate of A-210, P11 and P22 steels and concentration of dissolved O₂. Tests performed at A) pH 8.5 and 2 m/s; B) pH 8.5 and 3 m/s; C) pH 9.5 and 2 m/s; D) pH 9.5 and 3 m/s; E) pH 10 and 2 m/s; F) pH 10 and 3 m/s.

At pH 9.5, there was a considerable reduction on the corrosion rate to all three materials tested (Figure 4C and Figure 4D) with most of the values at around 0.05 mm/y

and some exception reaching 0.09 mm/y (Table 3). Similar than these results, Fujiwara et al.¹⁷ showed for the alkaline solution (pH 9.2) that the FAC rates decreased when dissolved

oxygen increased from 3 $\mu\text{g/L}$ to 10 $\mu\text{g/L}$. Furthermore, they showed that at 12 $\mu\text{g/L}$ of dissolved oxygen, the FAC rates were suppressed for all velocities tested.

At the highest pH, Figure 4E and Figure 4F, the corrosion rates were the lowest, with the majority of values below 0.03 mm/y.

Based on the general corrosion rates determined, it was decided that the sample images would be presented for the

most aggressive conditions tested: pH 8.5; 8 $\mu\text{g/L}$ of O_2 and 50 $\mu\text{g/L}$ of O_2 ; 2 m/s and 3 m/s. Figure 5 shows the images for the linear velocity of 2 m/s and Figure 6 shows the images for 3 m/s. As the corrosive processes were similar in the three samples, only one from each group tested is presented. As it can be seen in the images obtained before the weight loss tests, the coupons present dark corrosion products, a typical color of the magnetite layers (Fe_3O_4). These layers

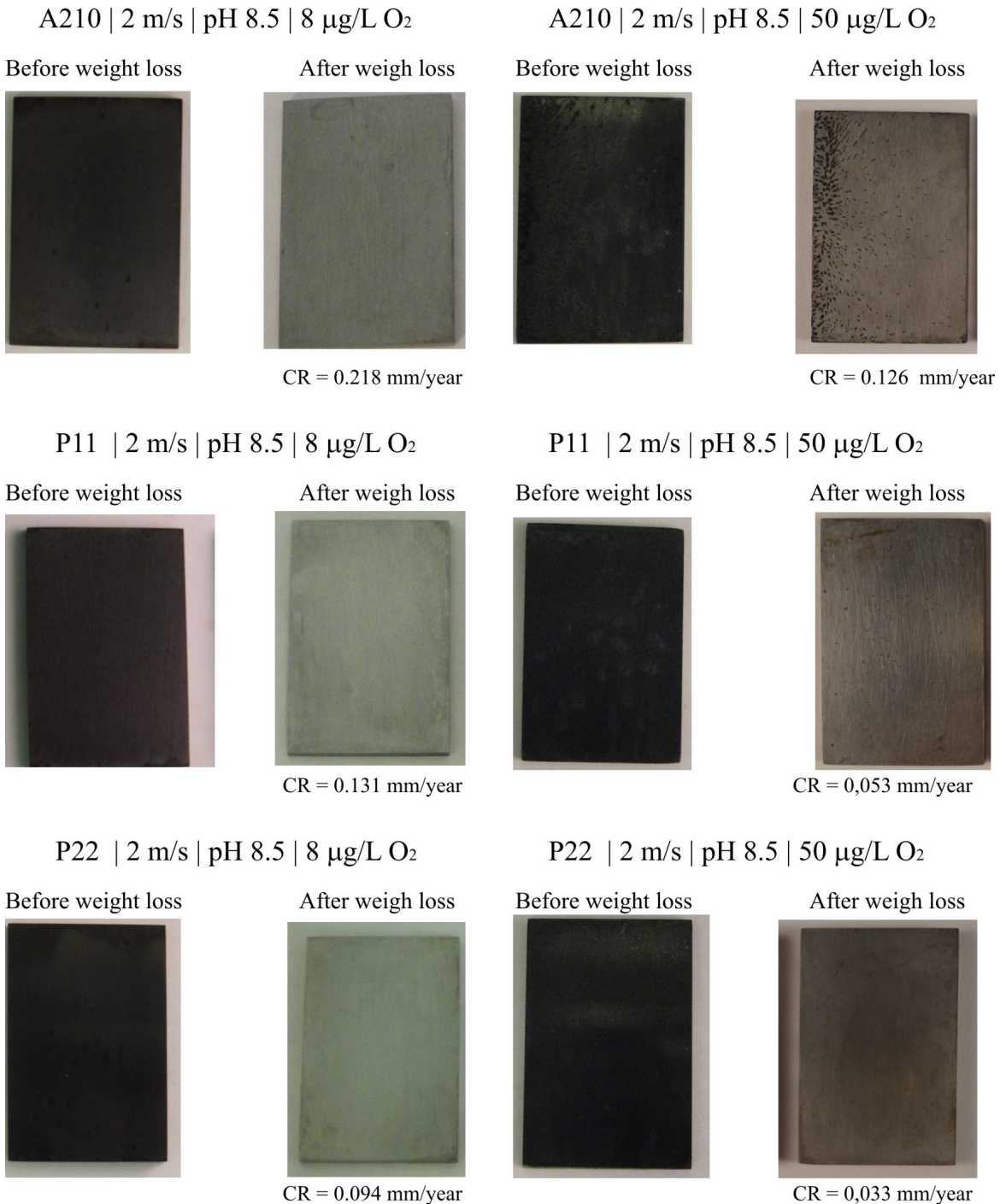


Figure 5. Images of A210, P11 and P22 steels tested at pH 8.5, 2 m/s, with 8 $\mu\text{g/L}$ O_2 and 50 $\mu\text{g/L}$ O_2 .

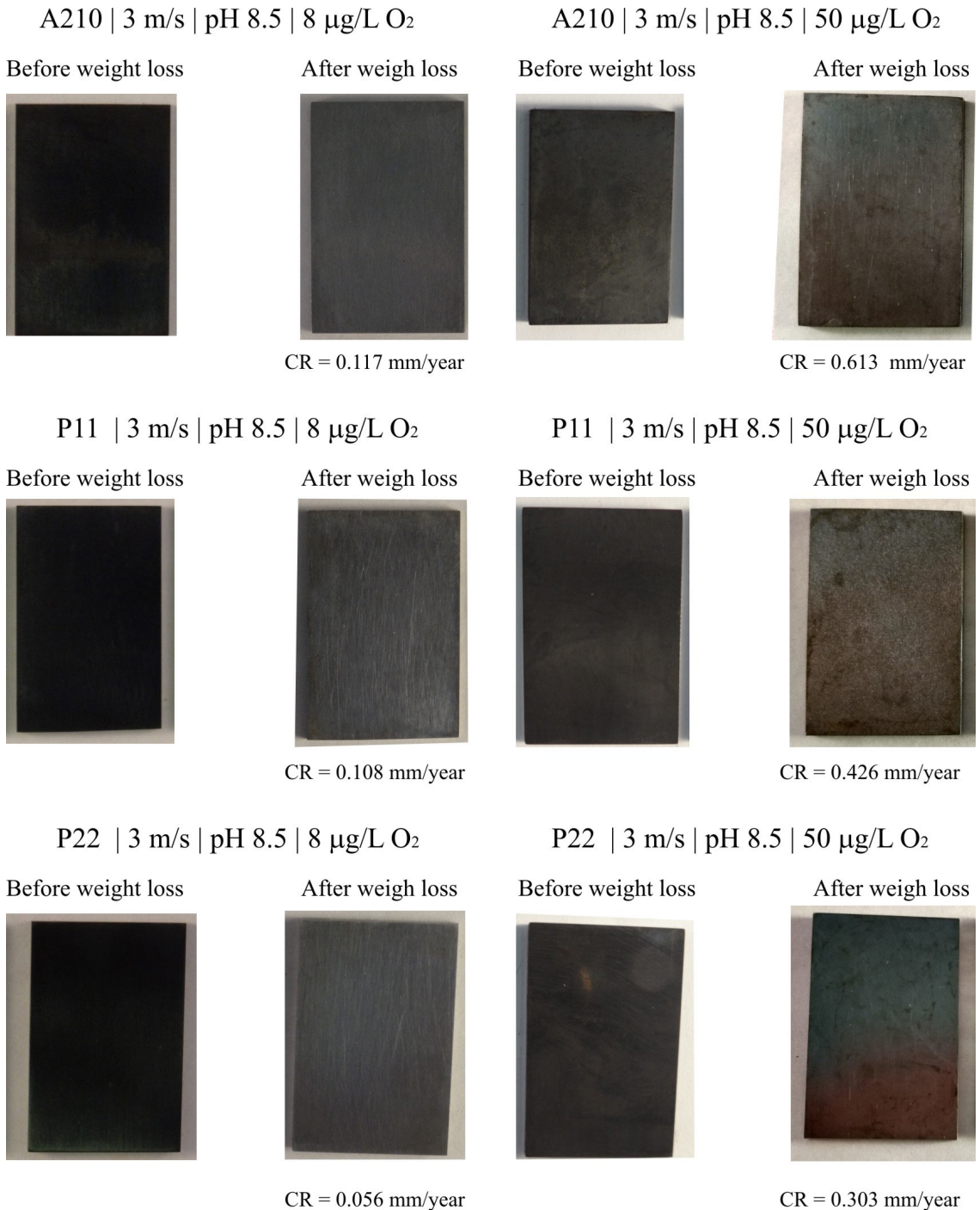


Figure 6. Images of A210, P11 and P22 steels tested at pH 8.5, 3 m/s, with 8 $\mu\text{g/L O}_2$ and 50 $\mu\text{g/L O}_2$.

were observed in all conditions and characterized by Raman Spectroscopy.

A surface analyses of carbon steel coupons before the weight loss were performed using a Raman confocal microscope. The corrosion products characterizations by Raman spectroscopy showed, therefore, predominantly heterogeneous layers, composed of maghemite ($\gamma\text{-Fe}_2\text{O}_3$) and magnetite (Fe_3O_4) corroborating with data from the

literature that indicate layers of semi-protective magnetite with the porosity filled with different Fe_2O_3 species^(2, 3, 18). Table 4 presents a summary of the layer compositions found in the coupons for all tests. Magnetite (Fe_3O_4) and maghemite ($\gamma\text{-Fe}_2\text{O}_3$) are the predominant oxide species whereas hematite ($\alpha\text{-Fe}_2\text{O}_3$) was identified in some coupons. However, magnetite always occurs in greater proportions. As described by Dooley and Lister¹⁸, maghemite ($\gamma\text{-Fe}_2\text{O}_3$)

Table 4. Composition of the corrosion layers by Raman Spectroscopy.

Testing Condition	Steel	Oxide Composition
2 m/s – pH 8.5 – 8 µg/L O ₂	A-210	γ-Fe ₂ O ₃ / α-Fe ₂ O ₃ / Fe ₃ O ₄
	P11	γ-Fe ₂ O ₃ / Fe ₃ O ₄
	P22	γ-Fe ₂ O ₃ / Fe ₃ O ₄
2 m/s – pH 8.5 – 50 µg/L O ₂	A-210	γ-Fe ₂ O ₃ / α-Fe ₂ O ₃ / Fe ₃ O ₄
	P11	γ-Fe ₂ O ₃ / Fe ₃ O ₄
	P22	γ-Fe ₂ O ₃ / Fe ₃ O ₄
3 m/s – pH 8.5 – 8 µg/L O ₂	A-210	γ-Fe ₂ O ₃ / Fe ₃ O ₄
	P11	γ-Fe ₂ O ₃ / Fe ₃ O ₄
	P22	γ-Fe ₂ O ₃ / α-Fe ₂ O ₃ / Fe ₃ O ₄
3 m/s – pH 8.5 – 50 µg/L O ₂	A-210	γ-Fe ₂ O ₃ / α-Fe ₂ O ₃ / Fe ₃ O ₄
	P11	γ-Fe ₂ O ₃ / α-Fe ₂ O ₃ / Fe ₃ O ₄
	P22	γ-Fe ₂ O ₃ / α-Fe ₂ O ₃
2 m/s – pH 9.5 – 8 µg/L O ₂	A-210	γ-Fe ₂ O ₃ / Fe ₃ O ₄
	P11	γ-Fe ₂ O ₃ / Fe ₃ O ₄
	P22	γ-Fe ₂ O ₃ / Fe ₃ O ₄
2 m/s – pH 9.5 – 50 µg/L O ₂	A-210	γ-Fe ₂ O ₃ / α-Fe ₂ O ₃ / Fe ₃ O ₄
	P11	γ-Fe ₂ O ₃ / α-Fe ₂ O ₃ / Fe ₃ O ₄
	P22	γ-Fe ₂ O ₃ / α-Fe ₂ O ₃ / Fe ₃ O ₄
3 m/s – pH 9.5 – 8 µg/L O ₂	A-210	γ-Fe ₂ O ₃ / Fe ₃ O ₄
	P11	γ-Fe ₂ O ₃ / Fe ₃ O ₄
	P22	γ-Fe ₂ O ₃ / Fe ₃ O ₄
3 m/s – pH 9.5 – 50 µg/L O ₂	A-210	Fe ₃ O ₄
	P11	α-Fe ₂ O ₃ / Fe ₃ O ₄
	P22	α-Fe ₂ O ₃ / Fe ₃ O ₄
2 m/s – pH 10 – 8 µg/L O ₂	A-210	γ-Fe ₂ O ₃ / Fe ₃ O ₄
	P11	γ-Fe ₂ O ₃ / Fe ₃ O ₄
	P22	γ-Fe ₂ O ₃ / Fe ₃ O ₄
2 m/s – pH 10 – 50 µg/L O ₂	A-210	γ-Fe ₂ O ₃ / Fe ₃ O ₄
	P11	γ-Fe ₂ O ₃ / Fe ₃ O ₄
	P22	γ-Fe ₂ O ₃ / Fe ₃ O ₄
3 m/s – pH 10 – 8 µg/L O ₂	A-210	γ-Fe ₂ O ₃ / Fe ₃ O ₄
	P11	γ-Fe ₂ O ₃ / Fe ₃ O ₄
	P22	γ-Fe ₂ O ₃ / Fe ₃ O ₄
3 m/s – pH 10 – 50 µg/L O ₂	A-210	γ-Fe ₂ O ₃ / Fe ₃ O ₄
	P11	γ-Fe ₂ O ₃ / α-Fe ₂ O ₃ / Fe ₃ O ₄
	P22	γ-Fe ₂ O ₃ / α-Fe ₂ O ₃

Maghemite (γ-Fe₂O₃) Hematite (α-Fe₂O₃) Magnetite (Fe₃O₄)

is often observed as an intermediate in the oxidation of magnetite to hematite. The magnetite (Fe₃O₄) typical bands²⁰ were at 306 cm⁻¹, 545 cm⁻¹ and 670 cm⁻¹; maghemite (γ-Fe₂O₃): at 340 cm⁻¹, 495 cm⁻¹, 662 cm⁻¹ and 700 cm⁻¹ and hematite (α-Fe₂O₃): at 215 cm⁻¹, 280 cm⁻¹, 390 cm⁻¹, 495 cm⁻¹, 590 cm⁻¹ and 1340 cm⁻¹.

3.2. Localized corrosion

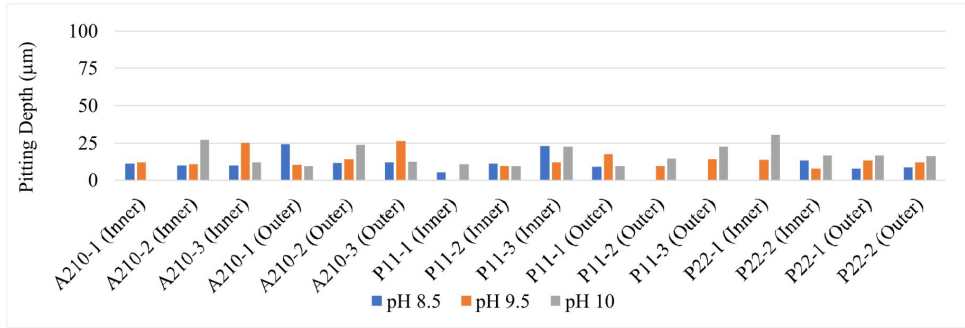
After the weight loss tests, all samples were analyzed by 3D confocal microscopy. The two sides of each sample, outer and inner in respect of center of cage, were analyzed with a magnitude of 100 times. Very few pits were found in each

coupon. However, despite of the reduced number of events, pits were always present. The depth of the most relevant pits is shown for each steel in the graphs of Figures 7 and 8. For 2 m/s and 3 m/s, both in the O₂-free environments and in those containing 8 µg/L of O₂, the pits had very low depths, below 25 µm, with a few events exceeding this value, reaching 40 µm. By increasing the concentration of dissolved O₂ to

50 µg/L, deeper pits were found, reaching values of up to 97 µm in P11 steel at pH 9.5, for both velocities. Thus, the concentration of dissolved O₂ proved to be the most relevant parameter for localized corrosion, generating the deepest pits when a higher concentration was used.

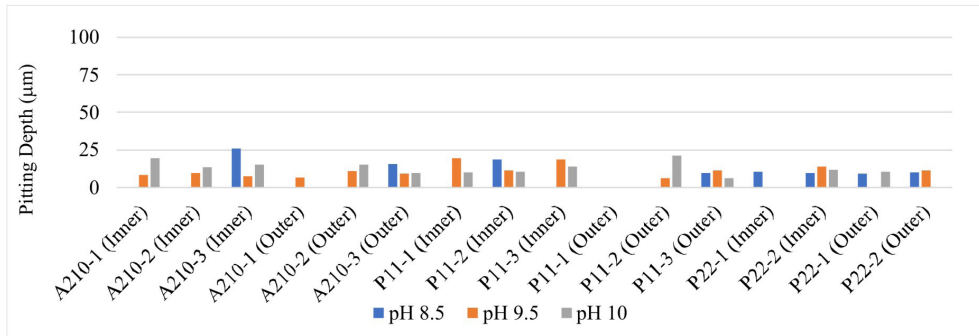
When comparing the localized corrosion results for the two linear velocities studied, with 50 µg/L O₂, we observed

2 m/s | 0 µg/L O₂



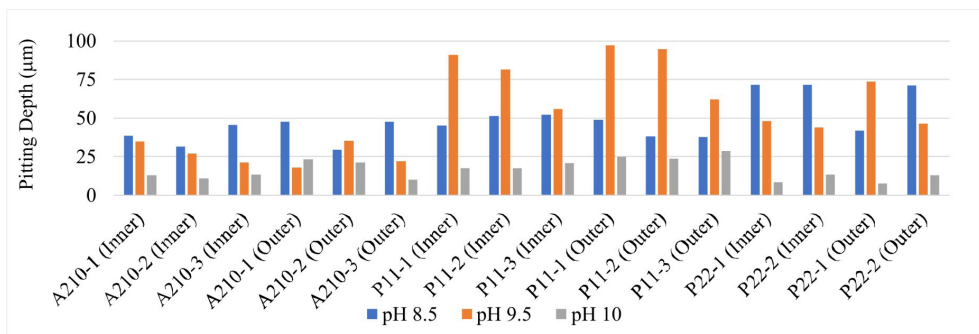
A

2 m/s | 8 µg/L O₂



B

2 m/s | 50 µg/L O₂



C

Figure 7. Pitting depth for A-210, P11 and P22 steels for tests with linear velocity of 2 m/s at different pH and dissolved O₂ concentration of: A) 0 µg/L O₂; B) 8 µg/L O₂ and C) 50 µg/L O₂.

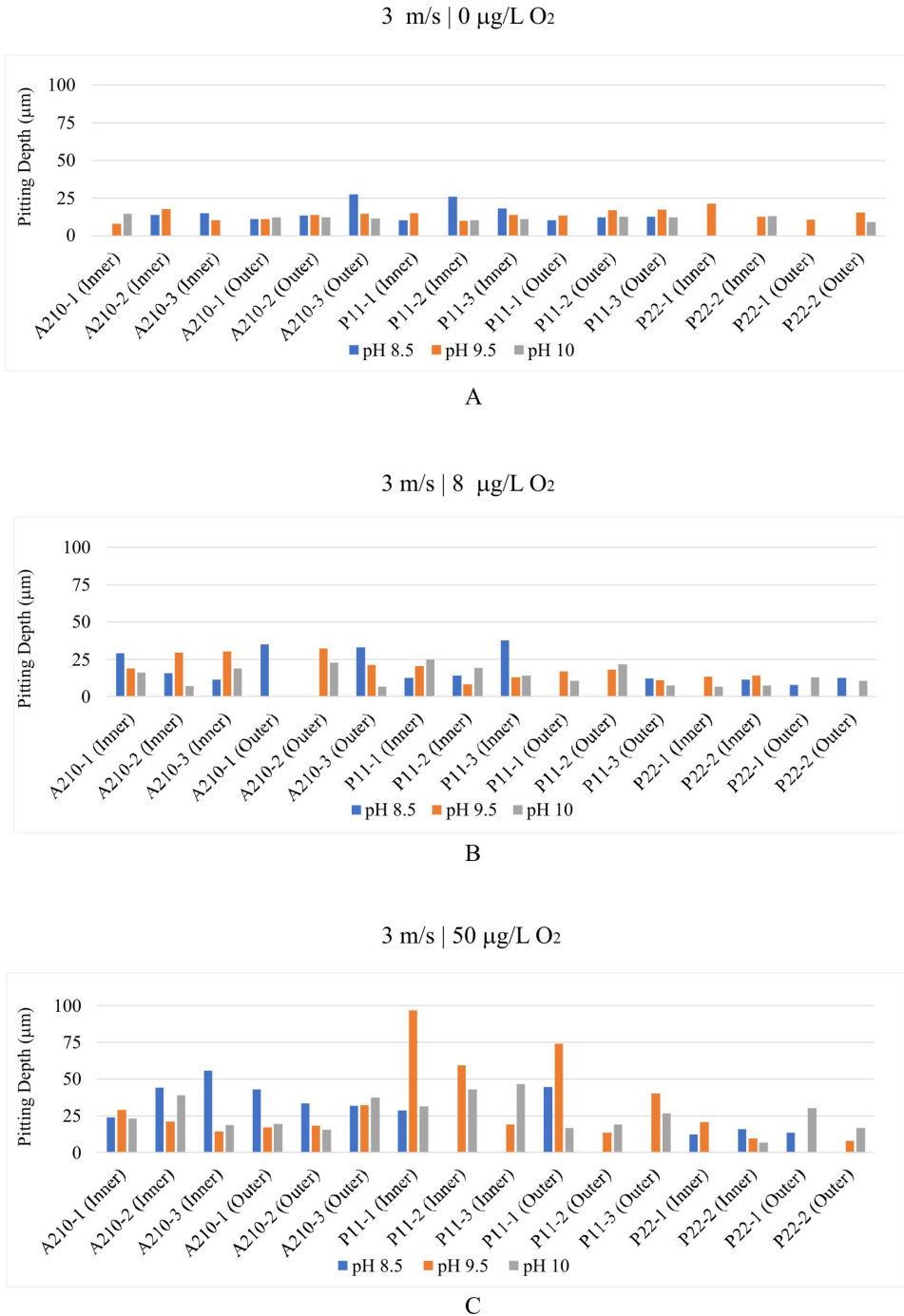


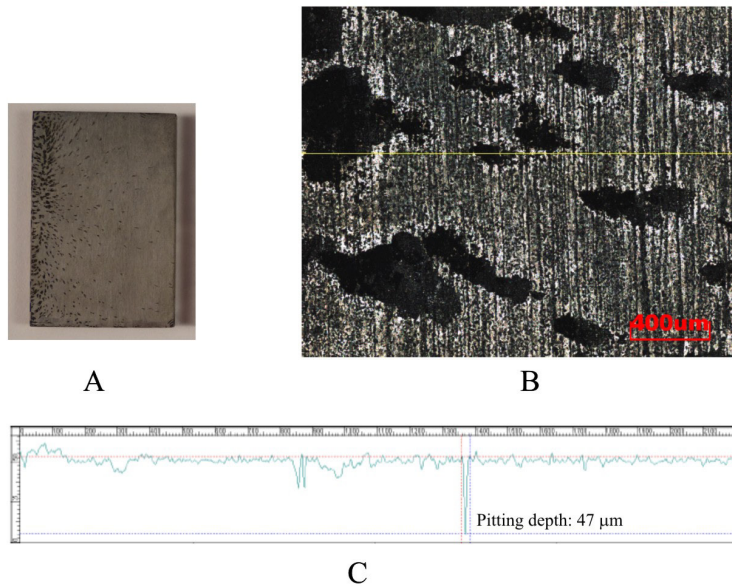
Figure 8. Pitting depth for A-210, P11 and P22 steels for tests with linear velocity of 3 m/s at different pH and dissolved O_2 concentration of: A) 0 $\mu\text{g/L O}_2$; B) 8 $\mu\text{g/L O}_2$ and C) 50 $\mu\text{g/L O}_2$.

the deepest events on tests performed at pH 9.5 which suggest that by decreasing general corrosion, as shown earlier (Table 3), the localized corrosion have become more evident.

The surface analyses of the most important events in the confocal microscope are shown in Figures 9 and 10. For the velocity of 2 m/s, Figure 9, both A-210 steel at pH 8.5 (A and B) and P11 steel at pH 9.5 (D and E) showed localized attacks distributed on the surface of the samples revealing the flow lines of the Rotating Cage system.

By analyzing the sample profile of the A-210 (C), yellow line of the image (B), the spots observed were quite shallow, having only one point with a relevant event with a depth of 47 μm . For the P11 steel, the observed events were deeper, with magnitudes of approximately 97 μm , as it can be seen by analyzing the profile (F). As for the velocity of 3 m/s, Figure 10, the images for A-210 steel at pH 8.5 (A and B) and P11 steel at pH 9.5 (D and E) did not show the flow lines as in 2 m/s. However, pits were observed during the

A210 | 2 m/s | pH 8.5 | 50 µg/L O₂



P11 | 2 m/s | pH 9.5 | 50 µg/L O₂

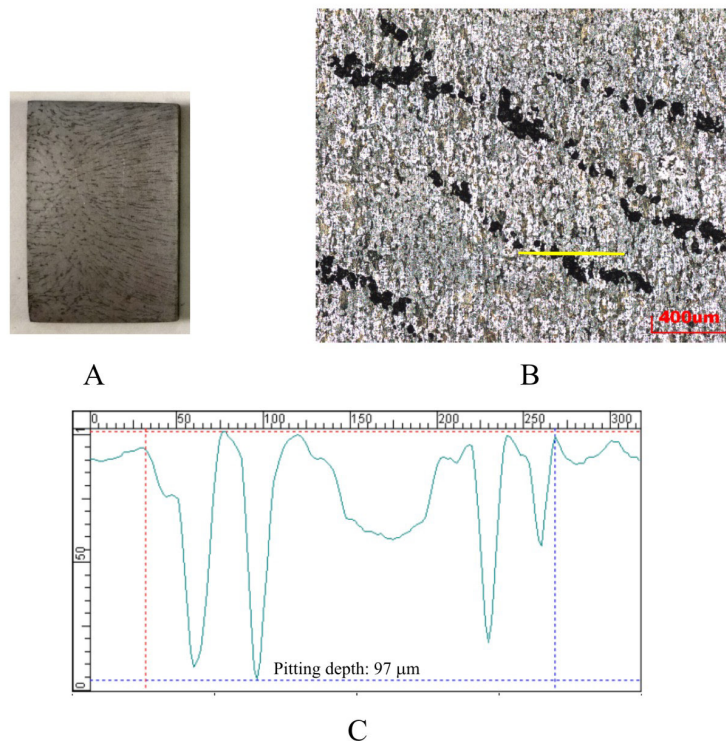


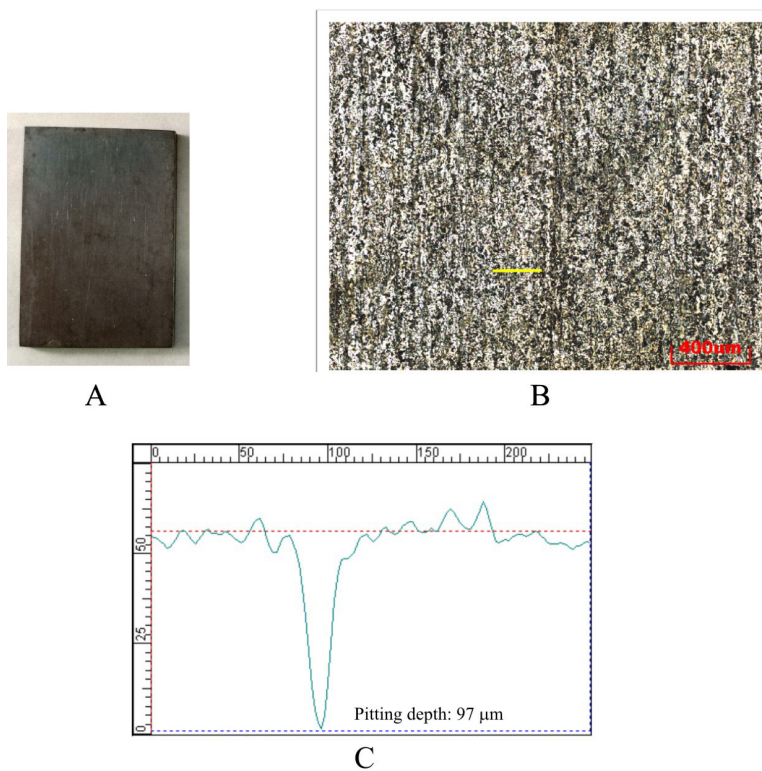
Figure 9. Surface analysis. ➤ A-210 steel – 2 m/s - pH 8.5 - 50 µg/L O₂ (A) coupon image; (B) micrograph; (C) profile analysis. ➤ P11 steel – 2 m/s - pH 9.5 - 50 µg/L O₂ (D) coupon image; (E) micrograph; (F) profile analysis.

profile analysis and with depths of 55 µm for the A-210 (C) and 96 µm for the P11 (F).

It is important to highlight that the deepest pits found in the media containing 50 µg/L the O₂, makes the extrapolations made from the weight losses to general corrosion rates inaccurate. This analysis should be done with great caution.

The pits shapes were classified as elliptical, which are considered less damaging to the structures of tubes and equipment. However, ongoing studies in our laboratory, with linear velocities greater than 3 m/s, have shown pits with narrow and deep shapes, typical of the accelerated flow corrosion (FAC) for these materials.

A210 | 3 m/s | pH 8.5 | 50 $\mu\text{g/L O}_2$



P11 | 3 m/s | pH 9.5 | 50 $\mu\text{g/L O}_2$

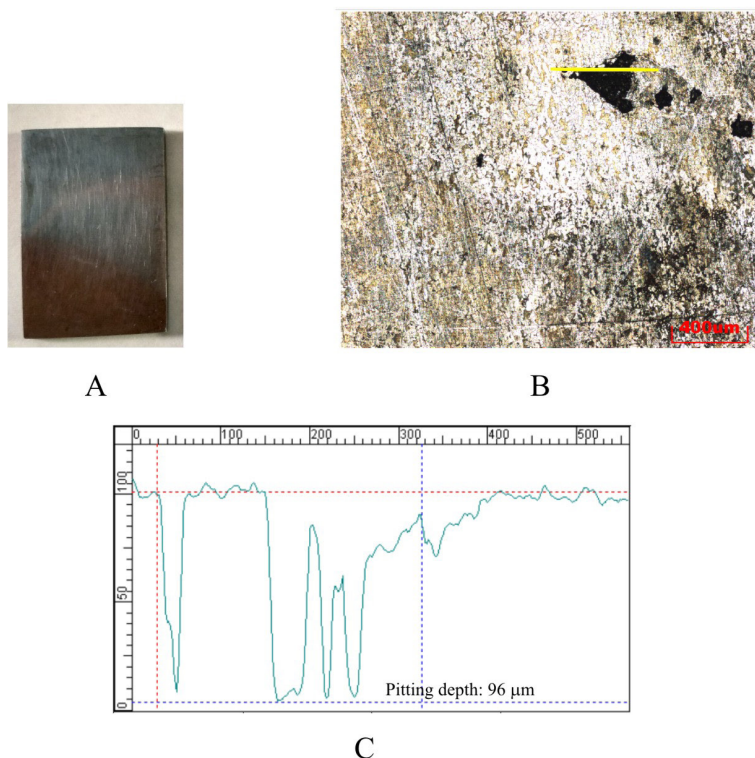


Figure 10. Surface analysis. > A-210 steel – 3 m/s - pH 8.5 - 50 $\mu\text{g/L O}_2$ (A) coupon image; (B) micrograph; (C) profile analysis. > P11 steel – 3 m/s - pH 9.5 - 50 $\mu\text{g/L O}_2$ (D) coupon image; (E) micrograph; (F) profile analysis.

4. Conclusions

The study of the influence of oxygen concentration, linear velocity and pH using a Rotating Cage system allowed a better understanding of Flow Accelerated Corrosion of the steels A-210, P11 and P22. The estimated general corrosion rates followed the order of magnitude: A-210 > P11 > P22. This behavior is associated with the effect of the chromium element on steel chemical composition. For pH 8.5 and linear velocity of 2 m/s, the highest general corrosion rates were observed on tests with 8 µg/L of dissolved O₂, decreasing the environment corrosivity with an increase in O₂ concentration to 50 µg/L. This was not observed in 3 m/s and pH 8.5, in which the corrosion rate increased when the dissolved O₂ content was increased. This evidenced the effect of the shear stress parameter on flow accelerated corrosion. In the other pH values, the effect of velocity was less significant.

The corrosion products characterization by Raman spectroscopy have shown heterogeneous layers for the three types of steel, basically composed of maghemite (γ-Fe₂O₃) and magnetite (Fe₃O₄), the latter being the main component for most of the conditions tested. Hematite (α-Fe₂O₃) was also observed in some layers.

The surface analyses have shown a localized attack in the majority of coupons, however with very low number of pits. On coupons tested with 50 µg/L of dissolved O₂ the deepest pits were found, imposing caution to extrapolations from weight loss data to corrosion rate.

In general, the results suggest that the ideal conditions to minimize the Flow Accelerated Corrosion (FAC) for these thermoelectric recovery boiler environments are: pH higher than 9.5 and dissolved O₂ concentration below 50 µg/L. P22 steel proved to be the most suitable material, with the lowest general corrosion rates and the incidence of the least damaging pits.

5. References

1. Shashidhar V, Patnail D. Flow accelerated corrosion in boilers/HRSGs. In: International Petroleum Technology Conference; 2015; Doha, Qatar. Proceedings. IPTC; 2015. (IPTC-18535-MS).
2. Dooley RB. Flow-accelerated corrosion in fossil plants and combined Cycle/HRSG plants. *Powerpl Chem*. 2008;10(2):68-89.
3. Dooley RB, Chexal VK. Flow-accelerated corrosion of pressure vessels in fossil plants. *Int J Press Vessels Piping*. 2000;77(2-3):85-90.
4. Ahmed WH. Evaluation of the proximity effect on flow-accelerated corrosion. *Ann Nucl Energy*. 2010;37(4):598-605.
5. Caravaggio M, Shulder S. Guidelines for control of flow-accelerated corrosion in fossil and combined cycle plants. Palo Alto: EPRI; 2017.
6. Vepsäläinen M, Saario T. Magnetite dissolution and deposition in NPP secondary circuit. Espoo: VTT; 2010. 44 p. (Research report; R-09735-10).
7. Kelley AD. Flow accelerated corrosion: detection and mitigation. In: CORROSION 2015; 2015; Houston, TX. Proceedings. Houston: NASE; 2015. (Paper; 5574).
8. Prasad M, Gopika V, Sridharan A, Parida S. Pipe wall thickness prediction with CFD based mass transfer coefficient and degradation feedback for flow accelerated corrosion. *Prog Nucl Energy*. 2018;107:205-14.
9. Prasad M, Gopika V, Sridharan A, Parida S, Gaikwad AJ. Hougaard process stochastic model to predict wall thickness in Flow Accelerated Corrosion. *Ann Nucl Energy*. 2018;117:247-58.
10. Yuan XX, Pandey MD, Bickel GA. A probabilistic model of wall thinning in CANDU feeders due to low-accelerated corrosion. *Nucl Eng Des*. 2008;238(1):16-24.
11. Rani HP, Divya T, Sahaya RR, Kain V, Barua DK. CFD study of flow accelerated corrosion in 3D elbows. *Ann Nucl Energy*. 2014;69:344-51.
12. Kain V. Flow accelerated corrosion: forms, mechanisms and case studies. *Procedia Eng*. 2014;86:576-88.
13. Kain V, Roychowdhury S, Ahmedabadi P, Barua DK. Flow accelerated corrosion: experience from examination of components from nuclear power plants. *Eng Fail Anal*. 2011;18(8):2028-41.
14. Trevin S. Nuclear corrosion science and engineering. Amsterdam : Elsevier; 2012. Chapter 7, Flow accelerated corrosion (FAC) in nuclear power plant components.
15. Dooley RB, Tilley R. Guidelines for controlling flow-accelerated corrosion in fossil and combined cycle plants. Palo Alto: EPRI; 2005.
16. Dillon JJ, Desch PB, Lai TS. The NALCO guide to boiler failure analysis. 2nd ed. New York: McGraw Hill Professional; 2011. Chapter 19, Flow-accelerated corrosion.
17. Fujiwara K, Yoneda K, Inada F. Effect of dissolved oxygen on flow-accelerated corrosion in neutral and alkaline solutions. In: EUROCORR; 2017; Prague, Czech Republic. Proceedings. Europe: European Federation of Corrosion; 2017. (Paper; 78701).
18. Dooley B, Lister D. Flow-Accelerated Corrosion in Steam Generating Plants. *Powerpl Chem*. 2018;20(4):194-244.
19. ASTM: American Society for Testing and Materials. ASTM G1-03: standard practice for preparing, cleaning, and evaluating corrosion test specimens. West Conshohocken: ASTM; 2011.
20. Faria DLA, Venâncio Silva S, Oliveira MT. Raman microspectroscopy of some iron oxides and oxyhydroxides. *J Raman Spectrosc*. 1997;28(11):873-8.